Preparation of Photoluminescence Tunable Cu-doped AgInS$_2$ and AgInS$_2$/ZnS Nanocrystals and Their Application as Cellular Imaging Probes

Siqi Chen[a,b], **Violeta Demillo**[a,b], **Minggen Lu**[c], and **Xiaoshan Zhu**[a,b,*]

[a]Department of Electrical and Biomedical Engineering, University of Nevada Reno, NV, USA

[b]Biomedical Engineering Program, University of Nevada Reno, NV, USA

[c]School of Community Health Sciences, University of Nevada Reno, NV, USA

Abstract

In this work, high-quality Cu doped AIS and AIS/ZnS NCs have been first synthesized via a surface doping approach. By varying Cu concentrations in doping, Cu doped AIS NCs exhibit a photoluminescence red-shift from around 600 nm to 660 nm with a decrease of quantum yield from around 30% to 20%. After ZnS coating or zinc etching on the Cu doped AIS NCs, Cu doped AIS/ZnS NCs present photoluminescence peaks from around 570 nm to 610 nm and high quantum yields in the range of 50 ~ 60%. Moreover, it is found that Cu doping can prolong the photoluminescence lifetime of NCs, and the average photoluminescence lifetime of Cu doped AIS and AIS/ZnS NCs is in the range of 300 ~ 500 ns. The resultant Cu doped AIS/ZnS NCs were further encapsulated with amphiphilic polymers and used as biocompatible photoluminescent probes in cellular imaging. The cellular imaging study shows that peptide-conjugated probes can specifically target U-87 brain tumor cells and thus they can be applied to the detection of endogenous targets expressed on brain tumor cells.

Graphical Abstract
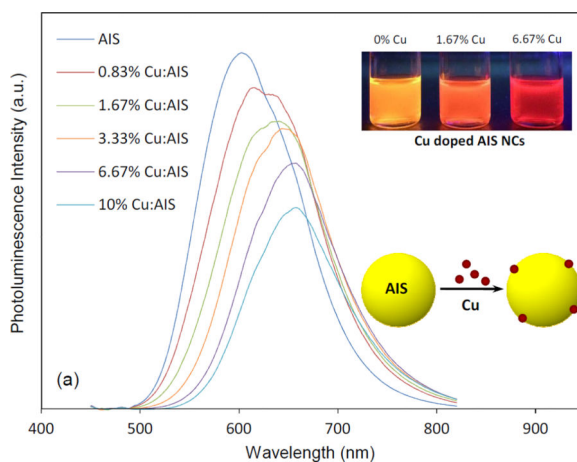
*To whom correspondence should be addressed. ; Email: xzhu@unr.edu. Phone: 1-775-682-6298. Fax: 1-775-784-6627

Photoluminescence tunable Cu-doped $AgInS_2$ and $AgInS_2/ZnS$ nanocrystals were synthesized and applied in cellular imaging.

INTRODUCTION

I–III–semiconductors nanocrystals (NCs) such as Cu-In-S (CIS) and Ag-In-S (AIS) and their core/shell CIS/ZnS and AIS/ZnS structures have been paid great attention due to their low toxicity and excellent composition-tunable electronic and optical properties.[1–10] They are emerging materials replacing the conventional cadmium-based NCs for optoelectronic and biomedical applications. For their preparation, thermal decomposition or heat up approaches are of particular interest because these approaches have the potential to be scaled up for low-cost mass production and thus provide sustainable and reliable materials for research and development.[4] Thermal decomposition for the synthesis of CIS has been successfully developed through simply heating copper iodide and indium acetate in dodecanethiol.[5] This approach is attractive because it can produce CIS NCs with tunable photoluminescence (PL) by controlling the NC growth time. The PL tuning of NCs is important for versatile applications. For instance, the PL of NCs can be tuned to avoid cross-talk with other existing dyes in bioimaging/sensing, and the PL tuning also can provide more design flexibility for optoelectronic devices such as light-emitting diodes (LEDs) with different color emissions. Moreover, in this approach, all precursors are commercially available and relatively safe to use (e.g., no glove box is needed in preparing these precursors, and no highly restricted handling or disposal is required). The synthesis of AIS NCs has also been reported by thermally decomposing $Ag_xIn_{1-x}(S_2CN(C_2H_5)_2)_4$ precursor.[6–8] To achieve different PL emissions, different precursors (with distinct Ag:In molar ratios) need to be prepared. However, the preparation of these precursors involves multiple wash/dry steps and the overall synthetic route is complex and time consuming. For AIS NCs, it is desired to develop a synthetic reaction similar to that for CIS NCs achieving both PL tuning and synthetic simplicity.

As shown in this work, we developed a heat-up approach using silver diethyldithiocarbamate and indium acetate in dodecanethiol and achieved bright AIS NCs. Although the reaction is simple, the PL of AIS NCs in such a reaction is almost fixed to yellow-orange (around 600 nm) and cannot be tuned with a prolonged NC growth time. Recent literature has shown that Cu doping into NCs has the capability to tune NC PL in a wide wavelength range.[11–25] For instance, Cu doped ZnS NCs show a pronounced red-shift in the PL peak position compared to the undoped ZnS host and present a blue-green emission depending on the doped Cu levels.[12] For CdS NCs, their green emission can be more extended to orange-red by Cu doping.[15] Green to red emissions have been achieved for Cu doped Zn-In-Se NCs.[18] Although the detailed mechanism of Cu doping for the PL tuning is not exactly clear, generally it is thought that Cu T_2 states are involved between conduction bands and valence bands of host NCs and responsible for the PL tuning.[20] Moreover, the PL tuning through Cu doping depends on the nature of host NCs.[11–25] Herein we report the use of Cu doping to tune the PL of AIS NCs. Briefly, after AIS NCs were synthesized via a heat-up approach, Cu precursors were dropwise introduced to the AIS NC solution for a surface doping. The PL of the prepared Cu doped AIS (Cu:AIS) NCs can be tuned from yellow to red by controlling

Cu concentration in the reaction. Although the PL quench was observed, the overall quantum yields (QYs) of NCs are still in the range of 20 ~ 30%. With two steps, the reaction is still scalable with simplicity (all precursors are commercially available and easy for handling and disposal). Further ZnS coating or zinc etching on Cu:AIS NCs has shown that the produced Cu:AIS/ZnS NCs can achieve QYs as high as 50 ~ 60%. It is also found that Cu doping can prolong the average PL lifetime of NCs, and the average PL lifetime of Cu:AIS and Cu:AIS/ZnS NCs is in the range of 300 ~ 500 ns. To our best knowledge, it is the first time to synthesize Cu:AIS and Cu:AIS/ZnS NCs and investigate the effect of Cu concentration on their optical properties.

In this study, the optical properties and material characteristics of Cu doped NCs have been characterized using PL spectroscopy, UV-Vis spectroscopy, X-ray diffraction (XRD), Transmission electron microscopy (TEM), Energy-dispersive X-ray (EDX) spectroscopy, and Time-resolved PL spectroscopy. The effects of Cu concentration on the doped NC optical properties were investigated and discussed. To explore and demonstrate the potential biomedical applications, Cu:AIS/ZnS NCs were encapsulated with amphiphiles and applied in cellular imaging as probes, and we performed cellular studies to investigate the probe cytotoxicity and specific cellular targeting/uptake of peptide-conjugated probes by brain tumor cells.

EXPERIMENTAL METHODS

Materials and Apparatus

Silver diethyldithiocarbamate (Ag(DDTC), 99.9%), indium (III) acetate (In(Ac)$_3$, 99.99%), and zinc stearate (ZnO: 12.5–14%) were purchased from Alfa Aesar. Copper(I) Iodide (CuI, 99.999%), sulfur (S, >99.99%), trioctylphospine (TOP, 90%), 1-dodecanethiol (DDT, 98%), 1-octadecene (ODE, 90%), acetone (>99%), methanol (99.93%), gelatin, and poly-D-lysine (PDL) were purchased from Sigma Aldrich. Tetrahydrofuran (THF, >99%), ethanol (>99%), chloroform (>99.9%), and hexane (95%) were purchased from Pharmco-AAPER. Fluorescein diacetate (FDA), propidium iodide (PI), 4',6-diamidino-2-phenylindole (DAPI) were from Pierce. U-87 MG (HTB-14) and HEK-293 cells (CRL-1537) were ordered from the American Type Culture Collection (ATCC). Roswell Park Memorial Institute (RPMI) 1640, Minimum Essential Medium (MEM) and Dulbecco's Modified Eagle Medium (DMEM) were from Corning Cellgro. Paraformaldehyde (PFA), phosphate buffered saline (PBS) and Dulbecco's phosphate buffered saline (DPBS) were from Fisher Scientific. Stempro accutase and heat-inactivated fetal bovine serum (FBS) were from Gibco. Bovine serum albumin (BSA) was from MP Biomedicals. RGD (Arg-Gly-Asp) and RAD (Arg-Ala-Asp) peptides were purchased from Peptides International. All chemicals or reagents were used as received without further purification.

The ultraviolet and visible (UV-Vis) spectra of materials were obtained with a UV-Vis spectrometer (UV-2450 from Shimadzu). PL spectra of NCs were acquired using a spectrophotometer (RF-5301PC from Shimadzu). Transmission electron microscope (TEM) images and Energy-dispersive X-ray (EDX) spectra were acquired using a JEOL analytical transmission electron microscope (model JEM 2100F operated with a 200 kV acceleration voltage) equipped with an Oxford Energy-Dispersive X-ray (EDX) spectrometer. X-ray

diffraction (XRD) data were collected by a coupled theta: 2-theta scan on a Rigaku Ultima-III diffractometer equipped with Copper X-ray tube with Ni beta filter, parafocusing optics, computer-controlled slits, and D/Tex Ultra 1D strip detector. Time-resolved PL lifetimes were measured by a Horiba Jobin Yvon Fluorolog-3 with a QY accessory and a time-correlated single-photon counting (TCSPC) spectrometer. The continuous excitation source was a 150 W ozone-free xenon arc-lamp. A pulsed xenon lamp or NanoLED (N-405L or N-300) was utilized as the excitation source for the PL decay measurement. Cells were imaged using a Leica confocal microscope and images were analyzed using ImageJ.

Synthesis of Cu:AIS NCs

Ag(DDTC) (0.1 mmol), In(Ac)$_3$ (0.2 mmol) and DDT (4 mL) were added in a three-necked round bottom flask equipped with a condenser and magnetic stir bar. This mixture was degassed under vacuum for 30 min at 125 °C until the solution became clear. The solution temperature was then increased to 190 ~ 200 °C under a flow of argon and held at this temperature for 10 min to grow AIS cores. After the reaction was completed, the solution was cooled to room temperature, and 4 mL of ODE was added to the AIS core growth solution without any purification. Then the solution was heated to 120 °C under vacuum for 20 min and then to 190 ~ 200 °C under argon. Copper precursors prepared by dissolving CuI (0.2 mmol) in DDT (8 mL) were injected into the solution for the formation of Cu:AIS NCs. After 10 min growth, the solution was cooled to room temperature. The NCs solution was purified repeatedly with the solvent combinations of hexane/ethanol and chloroform/acetone by centrifugation and then dried under vacuum. For the synthesis of Cu:AIS NCs with different Cu doping concentrations, the Cu initial concentrations ([Cu]/([Ag]+[In])) were changed in the range from 0 ~ 10 mol%. Small amounts of the reaction solution (0.1 ~ 0.2 mL) were collected using a syringe at different time intervals and injected into hexane in clean vials to terminate growth of NCs. All solutions collected from the experiment were diluted in a quartz cuvette with hexane for UV–Vis absorbance and PL measurements.

Synthesis of Cu:AIS/ZnS NCs

For ZnS shell growth, the zinc precursor was prepared by dissolving zinc stearate (0.4 mmol) in ODE (4 mL) at 140 °C, and the sulfur precursor was prepared by dissolving sulfur (0.4 mmol) in DDT (3.2 mL) and TOP (0.8 mL). The growth of the ZnS shell on Cu:AIS NCs was conducted *in situ* without purification of the core solution. Once the growth of cores was completed, the NCs solution was heated up to 210 °C under argon. Then both zinc and sulfur precursors were injected in sequence 3 times to the Cu:AIS growth solution in 0.5 mL portions at 15 min intervals. After the reaction was finished, mixtures were cooled down to room temperature and Cu:AIS/ZnS NCs were purified using hexane/ethanol and chloroform/acetone, and dried under vacuum.

QYs of NCs were calculated according to the following equation, using standard references including Rhodamine 6G (emission peak at 556 nm, QY = 95% in ethanol) and Oxazine 170 (emission peak at 640 nm, QY = 63% in methanol),

$$QY_S = QY_R \times (I_S/I_R) \times (A_R/A_S) \times (n_S/n_R)^2$$

where QY_S and QY_R are the quantum yields of sample and a standard reference, respectively; I_S and I_R are the integrations of fluorescence emissions of sample and a standard reference, respectively; A_S and A_R are the corresponding absorbance of sample and a standard reference, respectively; and n_S and n_R are the refractive indices of the corresponding solvents. In QY measurements, the absorbance of each sample or each standard reference deviated by less than 0.1. For each sample, the standard reference with the most similar absorption and/or luminescence characteristics was chosen for QY measurements.

Amphiphile-Encapsulated Cu:AIS/ZnS Micelles as Probes for Cellular Imaging

6.67% Cu:AIS/ZnS NCs were encapsulated using zwitterionic amphiphiles following what we reported previously.[26] Briefly, 2.4 mg Cu:AgInS2/ZnS NCs in THF (900 μL) and 1.6 mg zwitterionic amphiphiles in $CHCl_3$–MeOH (64 μL) were dispersed into water under sonication. After sonication, the organic solvents were removed by rotary evaporation at room temperature and the sample was filtered through a 0.2 μm syringe filter. Empty micelles or single-nanoparticle based micelles were removed by centrifugation at 18 000 rpm for 25 min. The collected micelles were dispersed in 400 μL of water as the micelle stock.

60 μL of the micelle stock was reacted with 0.3 mg RGD in borate buffer for 2 ~ 3 hours after the activation of carboxyl groups on micelles' surface using EDC/Sulfo-NHS. The RGD-conjugated micelles were washed by centrifugation, suspended in 200 μL borate, and stored at 4 °C before use as the conjugate stock. The same reaction was done for the conjugation of micelles with RAD peptide, and the RAD-conjugated micelles were used as a negative control. Non-conjugated micelles were also used as a control. A U-87 MG human brain glioblastoma cell line was cultured (37 °C, 5% CO_2) on glass coverslips coated with gelatin in MEM medium with 10% FBS until 50 ~ 80% confluency was achieved. The human embryonic kidney cell line HEK-293 was cultured (37 °C, 5% CO_2) on glass coverslips coated with PDL (poly-D-lysine) in RPMI-1640 medium with 10% FBS until 50 ~ 80% confluency was achieved. For the specific cell targeting study, cells were incubated with RGD-conjugated micelles in DMEM with 2% BSA at various concentrations or dilutions. As controls, cells were also incubated with RAD-conjugated micelles and non-conjugated micelles. After 3h incubation, cells were gently rinsed three times with PBS, fixed with 4% PFA in PBS solution for 20 minutes and washed three times with PBS. For cellular nuclei staining, cells were incubated with DAPI, washed three times with PBS, and then mounted on glass slides. Cells were imaged using a confocal microscope. Two-way ANOVA was applied to detect the differences among two cell lines. SAS (Statistical Analysis Software) 9.4 was used for data analysis.

RESULTS AND DISCUSSION

Cu atoms were doped into AIS NCs through a surface doping strategy – AIS NCs were first grown via thermal decomposition and then Cu precursors were injected into the AIS NC solution to react with AIS NCs. Figure 1(a) presents the effect of Cu concentrations on the PL spectra of Cu doped AIS NCs (Cu:AIS NCs). It can be seen that the PL peak wavelength

shows a continuous red shift from around 600 to 660 nm as Cu concentration in reaction is increased from 0 to 6.67% (molar percentage), and the red shift is not significant for Cu concentration above 6.67% or at 10%. The corresponding UV-vis absorption spectra of these Cu:AIS NCs are shown in Figure S1(a). As the Cu concentration increases, the absorbance edges of these samples are monotonously shifted to longer wavelength. The absorption edge of 10% Cu:AIS is similar to that of 6.67% Cu:AIS. This observation is consistent with their PL spectra. In Figure 1(a), it can also be seen that QYs of Cu:AIS NCs decrease from around 30% to 20% with the increase of Cu concentrations from 0% to 6.67%. QY of 10% Cu:AIS NCs even decrease further even though the PL is not red shifted. Through further comparing the PL spectra of Cu:AIS NCs, it can be seen that their shapes are also affected by Cu concentrations. The shape dependence on Cu concentration implicates that Cu atoms are incorporated into NC lattices and cause some changes of the lattice energy band or contribute to NC PL mechanisms. Of note, as shown in the inset of Figure 1(a), the PL of undoped or pure AIS NCs prepared in the thermal decomposition is hard to be tuned by the NC growth time. It can be seen that Cu doping is an effective way to tune NC PL.

The reason to adopt surface doping is that the optical property of NCs is more controllable than that using homogenous doping. With 3.33% Cu:AIS NCs as a demonstration, Figure 1(b) shows the evolution of their PL spectra in the time course of reaction through surface doping. It can be seen that around 45 nm red-shift occurs at 5 min after Cu injection. With further prolonged reaction time, no remarkable change in PL is observed with respect to peak wavelength and QY. The similar observation is also noticed in their absorption spectra as shown in Figure S1(b). This demonstrates that the Cu doping of AIS NCs is a fast and reliable process. However, with the same starting materials, if Cu precursor is mixed with silver and indium precursors in DDT for thermal decomposition, the PL of the produced NCs is observed to red shift to around 650 nm and then blue shift to around 600 nm, as shown in the inset of Figure 1(b). Moreover, the PL spectra become broader in the time course of reaction. It is possible that the final products could have both sub-populations of doped AIS NCs and undoped (or intrinsic) AIS NCs. Clearly, surface doping is a better approach to control the NC optical property.

To further understand the optical property of Cu:AIS NCs, these NCs were first characterized using XRD, TEM and EDX. Three representative samples (pure AIS, 1.67% Cu:AIS and 6.67% Cu:AIS) were investigated. As shown in Figure 2(a), the XRD pattern of the pure AIS NCs can be indexed with a tetragonal $AgInS_2$ crystal. Three apparent diffraction peaks observed at $2\theta = 26.8$, 44.7, and $52.6°$ can be assigned to diffractions from the (112), (204) and (312) planes of the tetragonal phase. Compared to the pure AIS NCs, diffraction patterns of Cu:AIS NCs slightly shifts to the higher angle side and approaches the 2θ values of the tetragonal $CuInS_2$ (CIS) along with the increase of Cu concentration. Since the ionic radius of Cu (0.74 nm) is smaller than that of Ag (1.14 nm), the observed shifts of the XRD patterns indicate the gradual replacement of Ag with Cu to form Cu:AIS NCs instead of forming individual CIS NCs.[27] These three samples were further characterized using TEM. Figure 2(b–d) present their TEM and high-resolution TEM (HRTEM) images. TEM images of AIS and Cu:AIS NCs show that their sizes are at 4 ~ 5 nm, indicating that the incorporation of Cu does not significantly influence the particle size. The HRTEM images show lattice plane spacings of 0.342, 0.340, and 0.332 nm for AIS, 1.67% Cu:AIS,

and 6.67% Cu:AIS NCs, respectively. The values of these spacings are corresponding to (112) planes determined from diffraction peaks at around 26–28 ° of XRD patterns in Figure 2(a). Both HRTEM and XRD data reveal that the obtained Cu:AIS NCs are not a mixture of individual AIS and CIS phases, but a Cu:AIS crystal. The energy dispersive X-ray (EDX) spectra (Figure S2) further confirms that AIS NCs are composed of Ag, In, and S and Cu:AIS NCs are composed of Cu, Ag, In and S. The resultant elemental compositions of AIS and Cu:AIS NCs are summarized in Table 1. For pure AIS NCs, the atomic ratio between Ag and In is close to 1:1. For Cu:AIS NCs, as Cu concentration is increased in the reaction, more Cu atoms are doped into NCs but the atomic percentage of Ag decreases. This observation indicates that Cu atoms enter the AIS structure and partially replace Ag atoms. The reason for the preferential substitution of Ag instead of In probably is that the Ag-S bond is weaker than the In-S bond.[28] More Cu atoms doped into NCs could cause more structure or surface defects quenching the NC PL for lower QYs. The EDX analysis of 10% Cu:AIS NCs was also conducted and the result shows that the element atomic ratio of Cu:Ag:In:S is 5.1:16.4:27.3:51.2. Compared to the element atomic ratio for 6.67% Cu:AIS NCs (as shown Table 1), more Cu atoms are observed in 10% Cu:AIS NCs. It is possible that the Cu level in AIS NCs may get saturated for 6.67% Cu:AIS NCs, and thus with a higher Cu concentration in doping, additional Cu atoms may be absorbed on NC surface to quench PL but not affect the position of PL peak.

It is known that ZnS coating on NCs can increase NC QY.[1] To enhance the PL QY, AIS and Cu:AIS NCs were passivated with a shell of ZnS to form AIS/ZnS and Cu:AIS/ZnS NCs. The QYs of AIS/ZnS, 1.67% Cu:AIS/ZnS and 6.67% Cu:AIS NCs are around 52.6%, 52.6%, 56.5% QYs, respectively. All of them present 30 ~ 50 nm blue shift in their PL spectra after ZnS coating. Figure 3(a) shows digital photographs of Cu:AIS and Cu:AIS/ZnS NCs suspended in organic solvents under a UV lamp. It can be seen that the emission colors of cores and core-shell structures are Cu-concentration dependent. Figure 3(b) demonstrates the typical PL and absorption spectra of 6.67% Cu:AIS NCs before and after ZnS coating. Figure 3(c) shows that the XRD diffraction pattern of the 6.67% Cu:AIS/ZnS NCs has a similar profile to that of 6.67% Cu:AIS cores, and shows a medium phase of Cu:AIS and ZnS crystals. The three main peaks shift to the high angle side and locate in the middle position of the pattern of Cu:AIS NCs and the standard pattern of cubic ZnS, which further suggests that Zn atoms are deposited or diffused to the surface of the Cu:AIS cores. Figure 3(d) shows the corresponding TEM and HRTEM images. The HRTEM image also reveals that the NCs have a clear lattice fringe with a plane spacing of 0.310 nm. The lattice planet spacing is close to that of the (111) plane in cubic ZnS NCs.[7] Similar to the core samples, Cu:AIS/ZnS NCs have a size around 4 ~ 5 nm. Probably, the ZnS coating is mainly dominated by zinc etching into core NCs. Figure S3 shows the EDX spectrum of 6.67% Cu:AIS/ZnS NCs. The elemental composition ratios of Cu, Ag, In, Zn, and S obtained from EDX analysis are 2.1%, 9.5%, 19.8%, 12.7%, and 55.8%, respectively. Both the atomic percentages of Ag and In decrease, however, the amount of Ag is reduced to a greater extent. At the same time, the atomic percentage of Zn is increased. The more reduction of Ag atomic percentage in Cu:AIS/ZnS NCs is probably due to Zn etching to preferentially replace Ag during the ZnS shell growth. We also notice that the Cu concentration in the core/shell structures is slightly lower than that of the Cu:AIS cores. Such results suggest that

in the Cu doping process, a portion of Cu atoms may sit on the surface of AIS cores and be replaced by zinc atoms during ZnS coating or zinc etching, and another portion of Cu atoms may diffuse into an inner layer of AIS lattice which cannot be replaced by zinc but still affect the PL of core/shell NCs.

Figures 4(a) shows the decay curves for AIS, 1.67% Cu:AIS, and 6.67% Cu:AIS NCs. Figure 4(b) presents the decay curves for their corresponding core/shell structures. For each decay curve, a biexponential function ($I(t) = A_1 e^{-t/\tau_1} + A_2 e^{-t/\tau_2}$) was used to fit the curve. τ_1 and τ_2 are the short and long lifetime parameters, respectively. A_1 and A_2 are the amplitudes of the decay components at t = 0. Table 2 lists the extracted characteristics parameters (τ_1, τ_2, A_1, and A_2) for all investigated samples. According to literature,[29–34] the PL lifetime parameters of AIS NCs could be associated with different electron-hole recombination pathways or mechanisms. After light excitation, electrons will be relaxed from conduction bands to surface trap states and donor states. The short lifetime is be attributed to electron transition from surface trap states (caused by surface defects) to valence bands. The long lifetime is attributed to electron transition from donor states to acceptor states, which results in the broad emission peaks of AIS NCs. From Table 2, it is observed that upon comparing A_1 parameter for each core and its corresponding core/shell structure, A_1 parameter is decreased and τ_1 is increased after ZnS shell growth. Considering the ZnS shell growth on each core causes QY enhancement, it is reasonable to attribute the decrease of A_1 to the minimization of surface defects. The prolonged τ_1 of core-shell structures probably is associated with electron transition from near-surface trap states or deep trap states to valence bands. The near-surface trap states or deep trap states could be closer to the donor states in energy levels and thus have a relatively longer lifetime for electrons. Upon examining the effect of Cu concentrations on A_1 and τ_1 of AIS cores, it can be seen that A_1 of Cu:AIS cores is decreased compared to that of undoped AIS cores. According to the literature model, the A_1 decrease should implicate the minimization of surface defects and thus the enhancement of QY upon Cu doping. However, Figure 1(a) show that Cu doping causes the decrease of QYs. Moreover, as shown in Figure 1(a), with low Cu concentrations, a shoulder in the PL spectrum is presented at the right side of the main PL peak. As Cu concentration increases, the shoulder is shifted to the left side of the main PL peak. As shown in Table 2, Cu doping also prolongs the average PL lifetime of NCs. It seems that although the literature model can well explain the effect of ZnS coating as well as some phenomena of undoped or intrinsic AIS NCs, a more sophisticated model or a different viewpoint is needed to explain the PL mechanisms of Cu:AIS NCs as well as the reason for the prolonged average PL lifetime upon Cu doping. According to literature,[24] the decrease of QYs with the increase of Cu doping levels is probably due to two reasons: (i) more defects in Cu:AIS lattice are created; (ii) high doping concentration causes closer distance between Cu atoms and cause strong Cu-Cu interaction and PL quenching. The transition/change of the PL spectrum shape versus Cu concentration in doping may be caused by multiple electron-hole recombination paths. According to literature,[20] Cu doping could introduce additional Cu T_2 states in the bandgap of AIS NCs. Meanwhile, our material characterization shows that Cu can etch and replace Ag in AIS host nanocrystals, and the doped Cu could form a Cu-In-S (CIS) layer on AIS surface. The formed CIS layer could possess some nature of CIS bandgap,[2] and new donor-acceptor pairs from CIS structures could be existing. The new CIS donor-acceptor

pairs also are energy levels incorporated in the bandgap of AIS hosts. On the other hand, AIS also has its own donor-acceptor pairs.[2–3] As a result, there could be several electron-hole recombination paths. The PL of nanocrystals should be a synergistic effect of all these recombination paths. Cu T_2 states and/or new CIS donor-acceptor pairs are Cu-concentration dependent, and thus gradually they can be more dominant than AIS donor-acceptor pairs as the Cu concentration increases in the doping process. As a result, we can see the change of the PL spectrum shape versus Cu concentration. With respect to the prolonged average PL lifetime, due to the incorporation of Cu T_2 states, the excited-state lifetime of the dopant emission is longer than the excitonic emission and the surface emission.[20] Thus, Cu doped nanocrystals gain a prolonged PL lifetime. The new CIS donor-acceptor pairs also are energy levels in the AIS bandgap and they could function as Cu T_2 states to prolong the average PL lifetime. Of note, these T_2 states and/or new CIS donor-acceptor pairs should be the causes for the emission at longer wavelengths (or red-shift in the doping process). Through this measurement on PL decay, it is also good to know that the average PL lifetime of the produced NCs is in the range of 300 ~ 500 ns. The NCs with long lifetimes are attractive for bioimaging – as bioimaging probes, they can be scanned using microscopy not only in regular intensity-based fluorescence mode but also in time-resolved fluorescence mode. Specifically, in the time-resolved mode, the long lifetime can distinguish NC fluorescence signals from the fast decaying autofluorescence in cells/tissue, and ensure NCs for more sensitive imaging.[35]

To demonstrate potential biomedical applications of Cu:AIS/ZnS NCs (i.e., specific targeting to brain tumor cells), we prepared micelles with 6.67% Cu:AIS/ZnS NCs and our previously reported zwitterionic amphiphiles through self-assembling. Human primary glioblastoma U-87 MG cells and human embryonic kidney 293 cells (HEK-293) are cell lines used in this study. The cytotoxicity of the micelles was first studied using these two cell lines. In the experiments, cells were incubated with micelles in growth medium with 10% FBS at various concentrations for 48 hr at 37 °C. After incubation, the growth medium was removed and the cells released from well bottom using stempro accutase, and then stained with FDA/PI to determine live vs dead cells using flow cytometry (Dead cells are red staining by PI and live cells are green staining by FDA). The cell viability was calculated as the ratio of live cells over the sum of live cells and dead cells. Figure S4 shows the measured cell viabilities for U-87 MG and HEK-293 after 48-hour incubation with micelles under different concentrations. It can be seen that for each cell line, the cell viabilities under all different micelle concentrations are around 95%, which are comparable to that of controls (no micelles in incubation). Thus the micelles loaded with Cu:AIS NCs are biocompatible. On the basis of the cytotoxicity study, these micelles were further conjugated with RGD and RAD peptides via EDC/Sulfo-NHS mediated reaction. RGD can specifically target to integrin $\alpha_v\beta_3$ overexpressed on U-87 MG cells and thus it is specific to U-87 MG cells. RAD with a molecular structure similar to RGD but is nonspecific to U-87 MG cells and thus used as a control.[36] HEK-293 not expressing integrin $\alpha_v\beta_3$ is used as a cell line control. In cellular uptake studies, each cell line was incubated with the RGD-conjugated micelles, RAD-conjugated micelles, and non-conjugated micelles under difference concentrations or dilutions in MEM medium with 2% BSA for 3 hours at 37 °C. After incubation, cells were gently rinsed three times with PBS, fixed with 4% PFA in PBS solution for 20 minutes and

washed three times with PBS. Afterwards, cells were incubated with DAPI for cellular nuclei staining, washed three times with PBS, and then mounted on glass slides. The mounted cells were then imaged using a Leica confocal microscope and images were analyzed using ImageJ. Figure 5 (A–F) shows representative cellular uptake images (overlaid confocal images) for U-87 and HEK-293. Quantitative data counting >100 cells for each experimental condition were presented in Figure 6. It can be seen that for each micelle concentration or dilution, U-87 cells internalize more RGD-conjugated micelles than HEK-293. RAD-conjugated and non-conjugated micelles had no significant cellular uptake by any of cell lines. Clearly, the micelles using Cu:AIS/ZnS NCs can be applied to the detection of endogenous targets expressed on brain tumor cells. In this study, the micelles were scanned in regular intensity-based fluorescence mode. We believe that they could be scanned in time-resolved fluorescence mode to achieve better image quality with respect to signal/noise ratio. In addition, radioactive ^{64}Cu may be doped into AIS NCs so that the achieved NCs have dual imaging functionalities for positron emission tomography (PET) and luminescence imaging.[37] Considering the hydrophobic core of micelles can also be loaded with both drugs and image contrasts, the specific cellular internalization suggests that the cadmium-free Cu:AIS/ZnS-micelles may also load drugs to be versatile nanoplatforms for cell- or tissue-based diagnosis and therapy.

CONCLUSION

In summary, high quality Cu:AIS and Cu:AIS/ZnS NCs have been successfully synthesized through a surface doping approach. The optical properties and material characteristics of Cu:AIS and Cu:AIS/ZnS NCs were studied with respect to Cu concentrations in reaction. It is found that Cu doping into AIS NCs can cause PL red-shift (from around 600 to 660 nm), PL quench (QYs from around 30% to 20%) and PL spectrum shape change as Cu concentration in reaction increases from 0 to 6.67%. After ZnS coating or zinc etching, Cu atoms were still observed in AIS/ZnS NCs playing a role in tuning PL of AIS/ZnS NCs (570 ~ 610 nm), and QYs of Cu:AIS/ZnS NCs are in the range of 50 ~ 60%. Moreover, Cu doping can prolong the PL lifetime of NCs, and the average PL lifetime of Cu doped AIS and AIS/ZnS NCs is in the range of 300 ~ 500 ns. To demonstrate their biomedical application, Cu:AIS/ZnS NCs were encapsulated with amphiphilic polymers and applied in cellular imaging as probes. The cellular study has shown that RGD-conjugated probes can be specifically targeted and internalized into U-87 brain tumor cells. Finally, besides the cellular imaging applications, we believe that Cu:AIS and Cu:AIS/ZnS NCs can find broad applications in solid-state lighting and photovoltaic devices due to their unique properties in PL wavelength tuning and high QYs.

Supplementary Material

Refer to Web version on PubMed Central for supplementary material.

Acknowledgments

REFERENCES

1. Xie R, Rutherford M, Peng X. J. Am. Chem. Soc. 2009; 131:5691. [PubMed: 19331353]

2. Zhong H, Bai Z, Zou B. J. Phys. Chem. Lett. 2012; 3:3167. [PubMed: 26296024]

3. Torimoto T, Kameyama T, Kuwabata S. J. Phys. Chem. Lett. 2014; 5:336. [PubMed: 26270709]

4. van Embden J, Chesman ASR, Jasieniak JJ. Chem. Mater. 2015; 27:2246.

5. Li L, Pandey A, Werder DJ, Khanal BP, Pietryga JM, Klimov VI. J. Am. Chem. Soc. 2011; 133:1176. [PubMed: 21207995]

6. Dai M, Ogawa S, Kameyama T, Okazaki KI, Kudo A, Kuwabata S, Tsuboi Y, Torimoto T. J. Mater. Chem. 2012; 22:12851.

7. Torimoto T, Adachi T, Okazaki KI, Sakuraoka M, Shibayama T, Ohtani B, Kudo A, Kuwabata S. J. Am. Chem. Soc. 2007; 129:12388. [PubMed: 17887678]

8. Torimoto T, Ogawa S, Adachi T, Kameyama T, Okazaki KI, Shibayama T, Kudo A, Kuwabata S. Chem. Commun. 2010; 46:2082.

9. Xiong W, Yang G, Wu X, Zhu J. ACS Appl. Mater. Interfaces. 2013; 5:8210. [PubMed: 23910957]

10. Xiong W, Yang G, Wu X, Zhu J. J. Mater. Chem. B. 2013; 1:4160.

11. Norris DJ, Efros AL, Erwin SC. Science. 2008; 28:1776. [PubMed: 18369131]

12. Corrado C, Hawker M, Livingston G, Medling S, Bridges F, Zhang JZ. Nanoscale. 2010; 2:1213. [PubMed: 20648352]

13. Karan NS, Sarma DD, Kadam RM, Pradhan N. J. Phys. Chem. Lett. 2010; 1:2863.

14. Mandal P, Talwar SS, Major SS, Srinivasa RS. J. Chem. Phys. 2008; 128:114703. [PubMed: 18361597]

15. Stouwdam JW, Janssen RA. Adv. Mater. 2009; 21:2916.

16. Shen H, Wang H, Li X, Niu JZ, Wang H, Chen X, Li LS. Dalton Trans. 2009; 10534

17. Jana S, Srivastava BB, Acharya S, Santra PK, Jana NR, Sarma DD, Pradhan N. Chem. Commun. 2010; 46:2853.

18. Sarkar S, Karan NS, Pradhan N. Angew. Chem. Int. Ed. 2011; 50:6065.

19. Xu S, Wang C, Wang Z, Zhang H, Yang J, Xu Q, Shao H, Li R, Lei Wei, Cui Y. Nanotechnology. 2011; 22:275605. [PubMed: 21597150]

20. Srivastava BB, Jana S, Pradhan N. J. Am. Chem. Soc. 2011; 133:1007. [PubMed: 21186798]

21. Zhang W, Zhou X, Zhong X. Inorg. Chem. 2012; 51:3579. [PubMed: 22364175]

22. Zhang W, Lou Q, Ji W, Zhao J, Zhong X. Chem. Mater. 2014; 26:1204.

23. Wang X, Yan X, Li W, Sun K. Adv. Mater. 2012; 24:2742. [PubMed: 22528857]

24. Zeng R, Shen R, Zhao Y, Sun Z, Li X, Zheng J, Cao S, Zou B. Cryst Eng Comm. 2014; 16:3414.

25. Zeng R, Shen R, Zhao Y, Li X, Sun Z, Shen Y. Nanotechnology. 2014; 25:135602. [PubMed: 24583650]

26. Demillo VG, Zhu X. J. Mater. Chem. B. 2015; 3:8328.

27. Ikeda S, Nakamura T, Harada T, Matsumura M. Phys. Chem. Chem. Phys. 2010; 12:13943. [PubMed: 20852813]

28. Delgado GE, Mora AJ. Chalcogenide Lett. 2009; 6:635.

29. Mao B, Chuang CH, Wang J, Burda C. J. Phys. Chem. C. 2011; 115:8945.

30. Ogawa T, Kuzuya T, Hamanaka Y, Sumiyama K. J. Mater. Chem. 2010; 20:2226.

31. Hamanaka Y, Ogawa T, Tsuzuki M, Kuzuya T. J. Phys. Chem. C. 2011; 115:1786.

32. Hamanaka Y, Ogawa T, Tsuzuki M, Ozawa K, Kuzuya T. J. Lumin. 2013; 133:121.

33. Hamanaka Y, Ozawa K, Kuzuya T. J. Phys. Chem. C. 2014; 118:14562.

34. Park YJ, Oh JH, Han NS, Yoon HC, Park SM, Do YR, Song JK. J. Phys. Chem. C. 2014; 118:25677.

35. Mandal G, Darragh M, Wang YA, Heyes CD. Chem. Commun. 2013; 493:624.

36. Choi HS, Gibbs SL, Lee JH, Kim SH, Ashitate Y, Liu F, Hyun H, Park G, Xie Y, Bae S, Henary M, Frangioni JV. Nature Biotech. 2013; 31:148.

37. Guo W, Sun X, Jacobson O, Yan X, Min K, Srivatsan A, Niu G, Kiesewetter DO, Chang J, Chen X. ACS Nano. 2015; 9:488. [PubMed: 25549258]
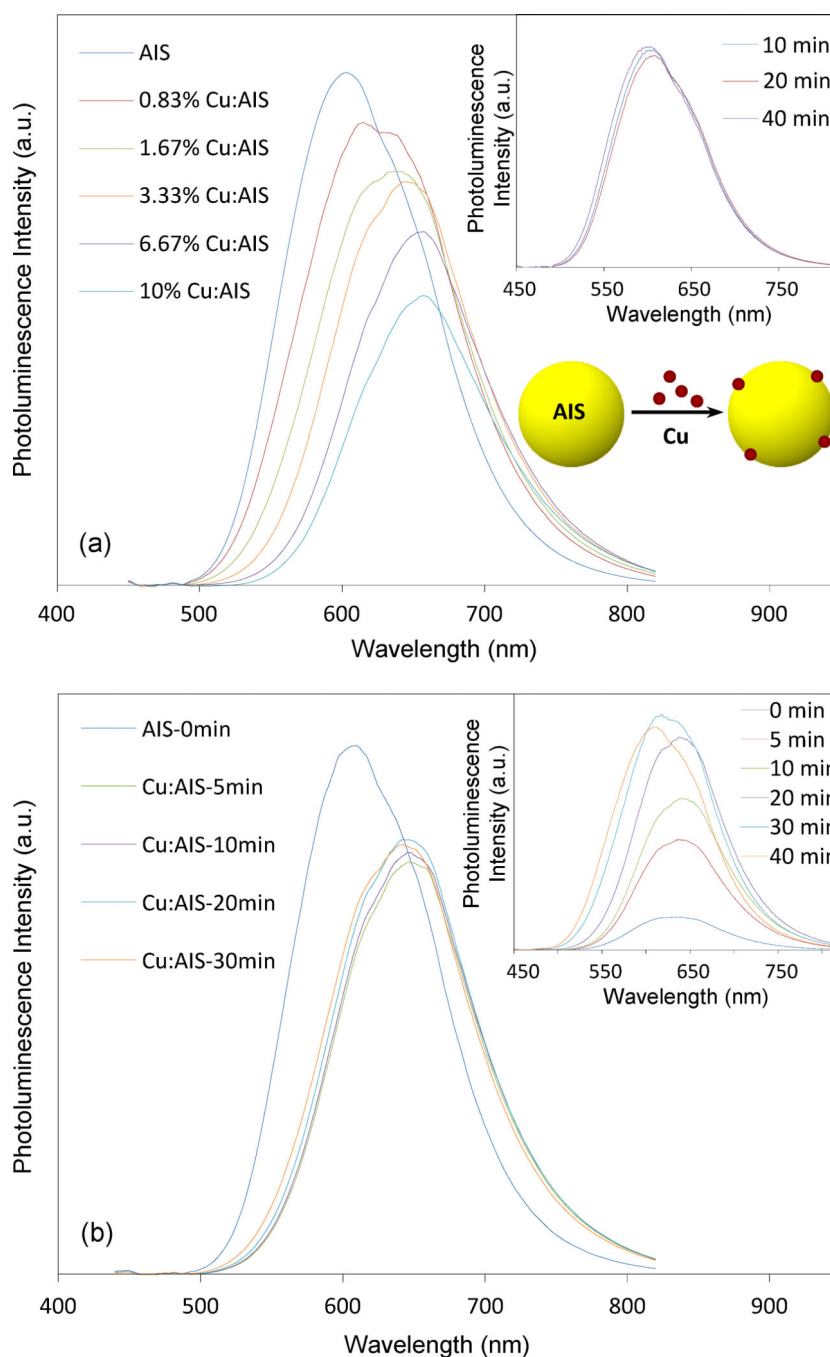
Figure 1.
(a) Effect of Cu concentrations in a surface doping strategy on the PL spectra of Cu: AIS (Cu:AIS) NCs. The inset data plot presents that the evolution of PL spectra of undoped AIS NCs is not significant in the time course of growth; and (b) Evolution of PL spectra of 3.33% Cu:AIS NCs in the time course of reaction using the surface doping approach. The inset is the evolution of PL spectra of Cu:AIS NCs prepared through a homogenous reaction (Cu precursor mixed with silver and indium precursors simultaneously in a thermal decomposition). Note that all PL spectra of NCs are scaled by their quantum yields.
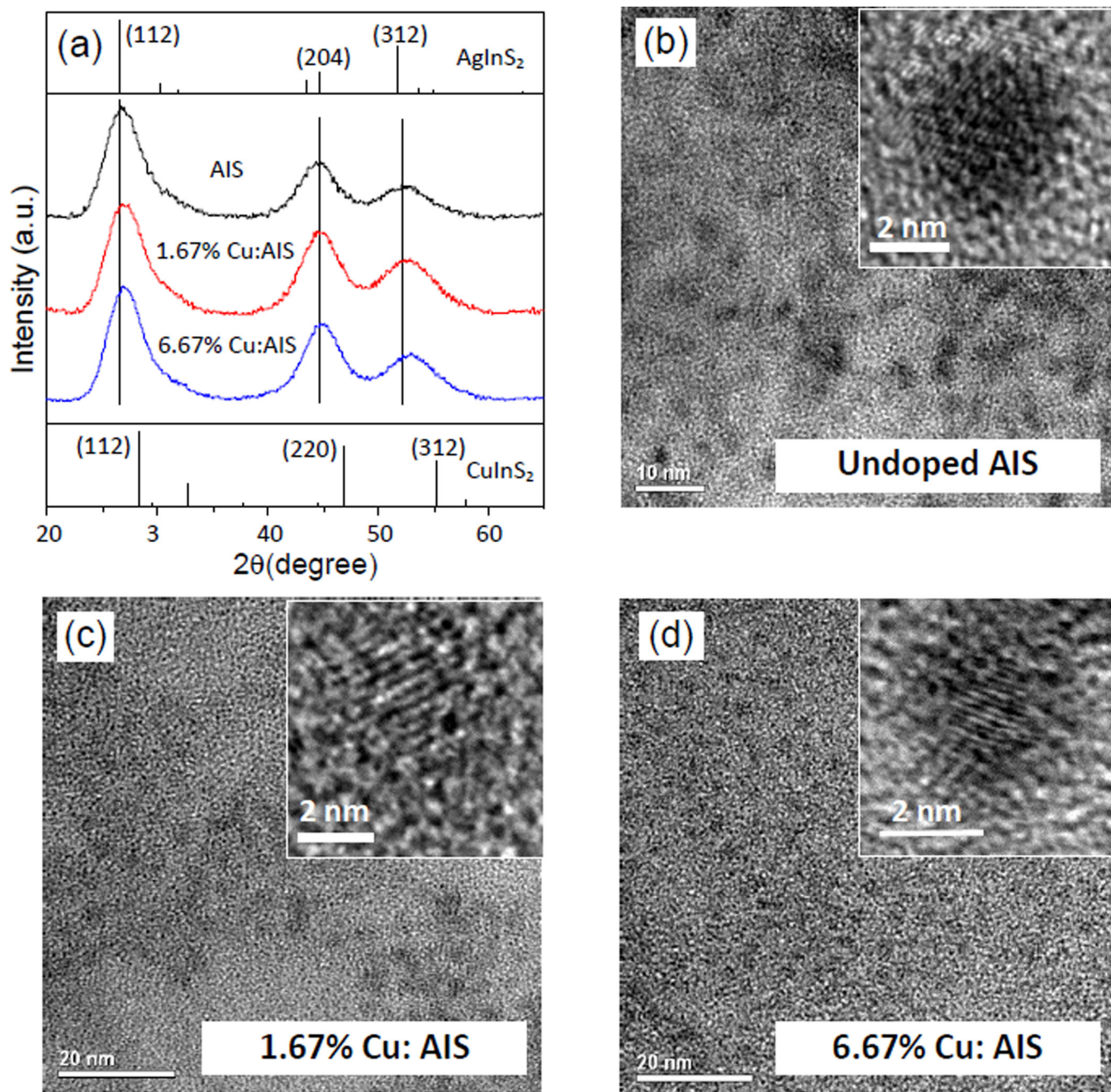
Figure 2.
(a) XRD patterns for AIS, 1.67% Cu:AIS and 6.67% Cu:AIS NCs. Diffraction peaks of tetragonal $AgInS_2$ and $CuInS_2$, as obtained from JCPDS #25-1330 and JCPDS #38-0777, are shown as references; and (b–d) TEM and high resolution TEM images of these NCs.
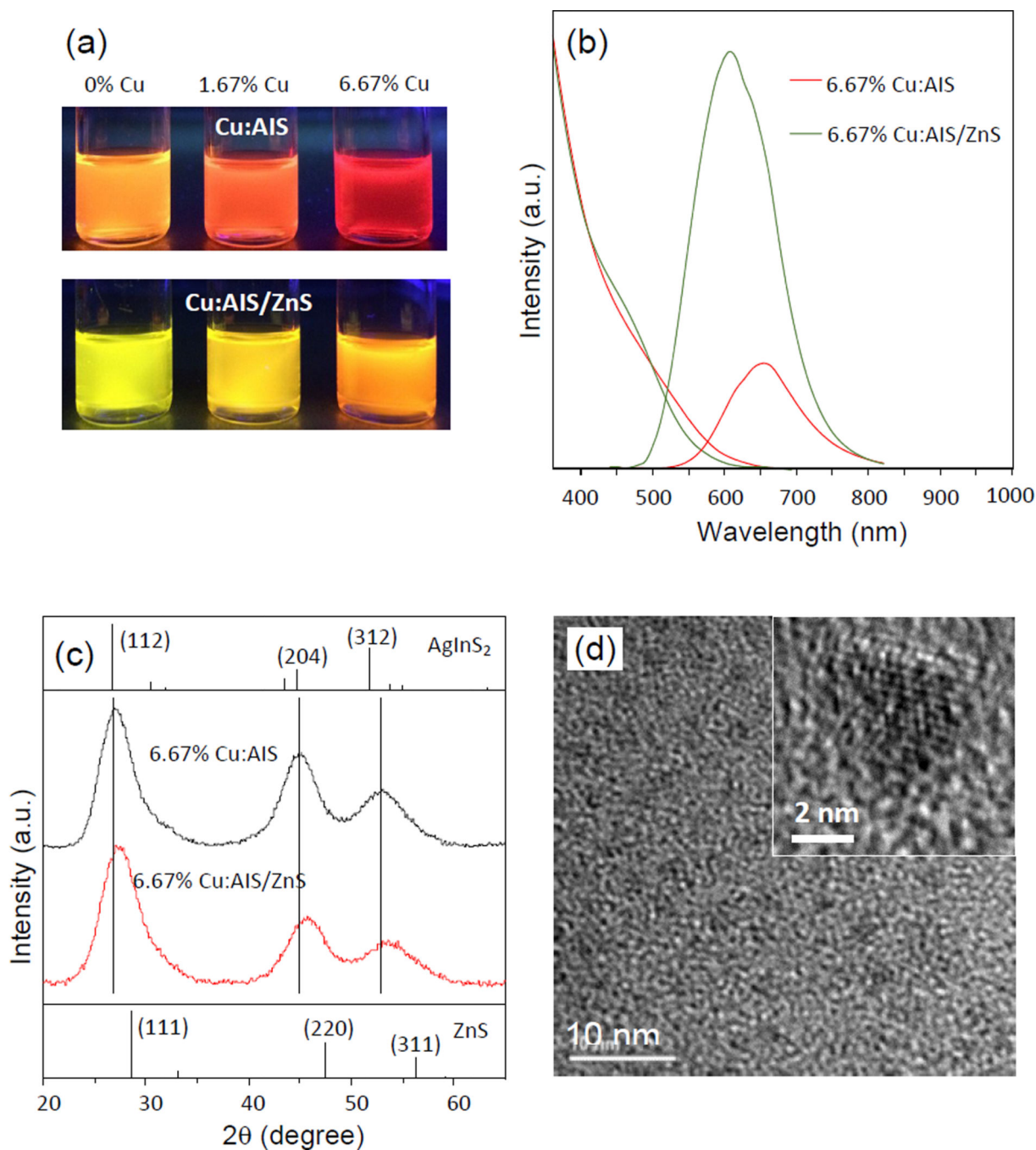
Figure 3.
(a) Digital photographs of Cu:AIS and Cu:AIS/ZnS NCs suspended in organic solvents under a UV lamp, (b) PL and absorption spectra of 6.67 % Cu:AIS and Cu:AIS/ZnS NCs. All PL spectra of NCs are scaled by their quantum yields, (c) XRD patterns of 6.67 % Cu:AIS and Cu:AIS/ZnS NCs. Diffraction peaks of tetragonal $AgInS_2$ and ZnS, as obtained from JCPDS #25-1330 and JCPDS #05-0566, are shown as references, and (d) TEM and high resolution TEM images of 6.67 % Cu:AIS/ZnS NCs.
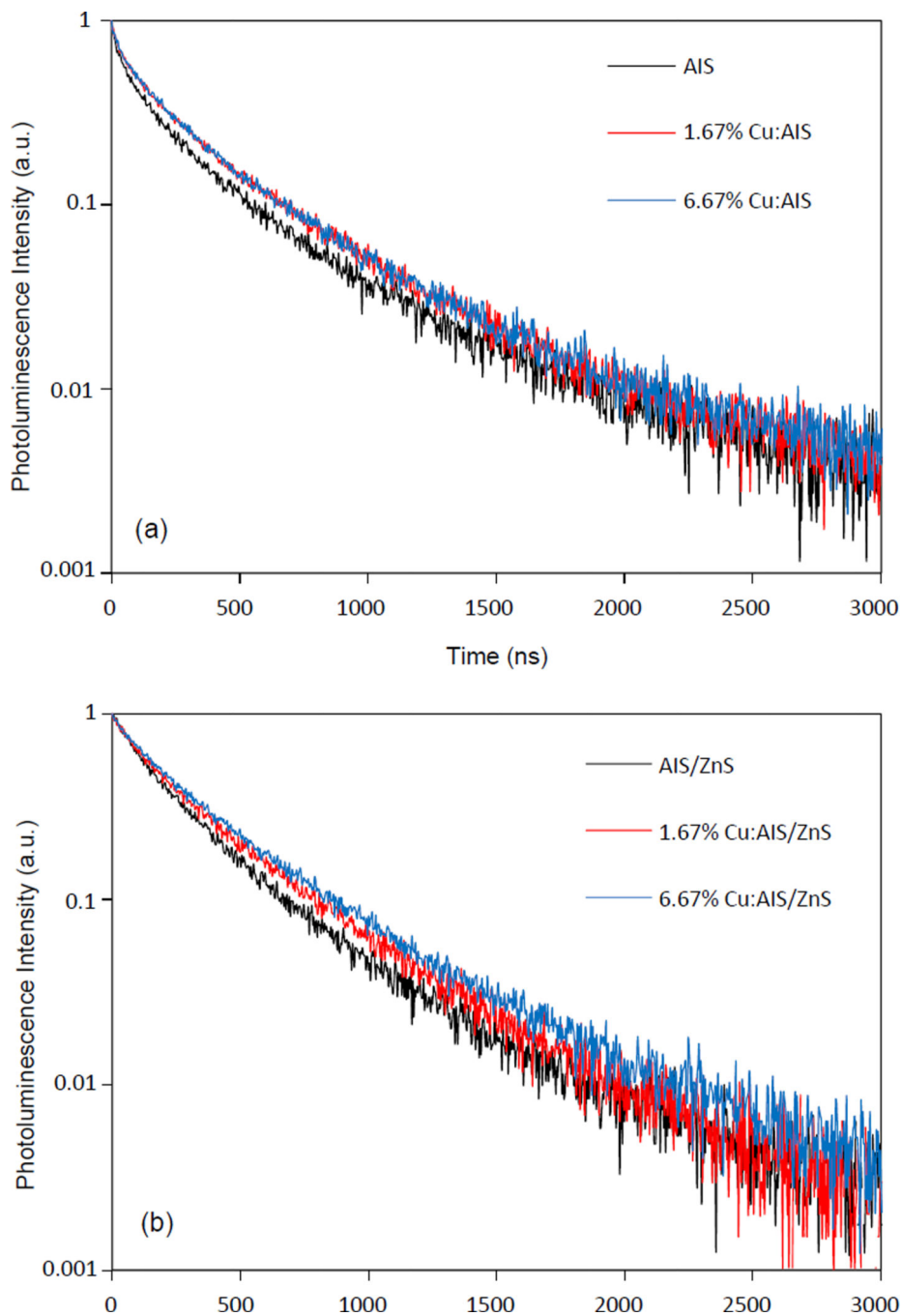
Figure 4.
(a) PL decay curves of Cu:AIS NCs, and (b) PL decay curves of the corresponding Cu:AIS/ZnS NCs. All samples were excited at 405 nm and the decay for each NC sample was measured at its PL peak wavelength.
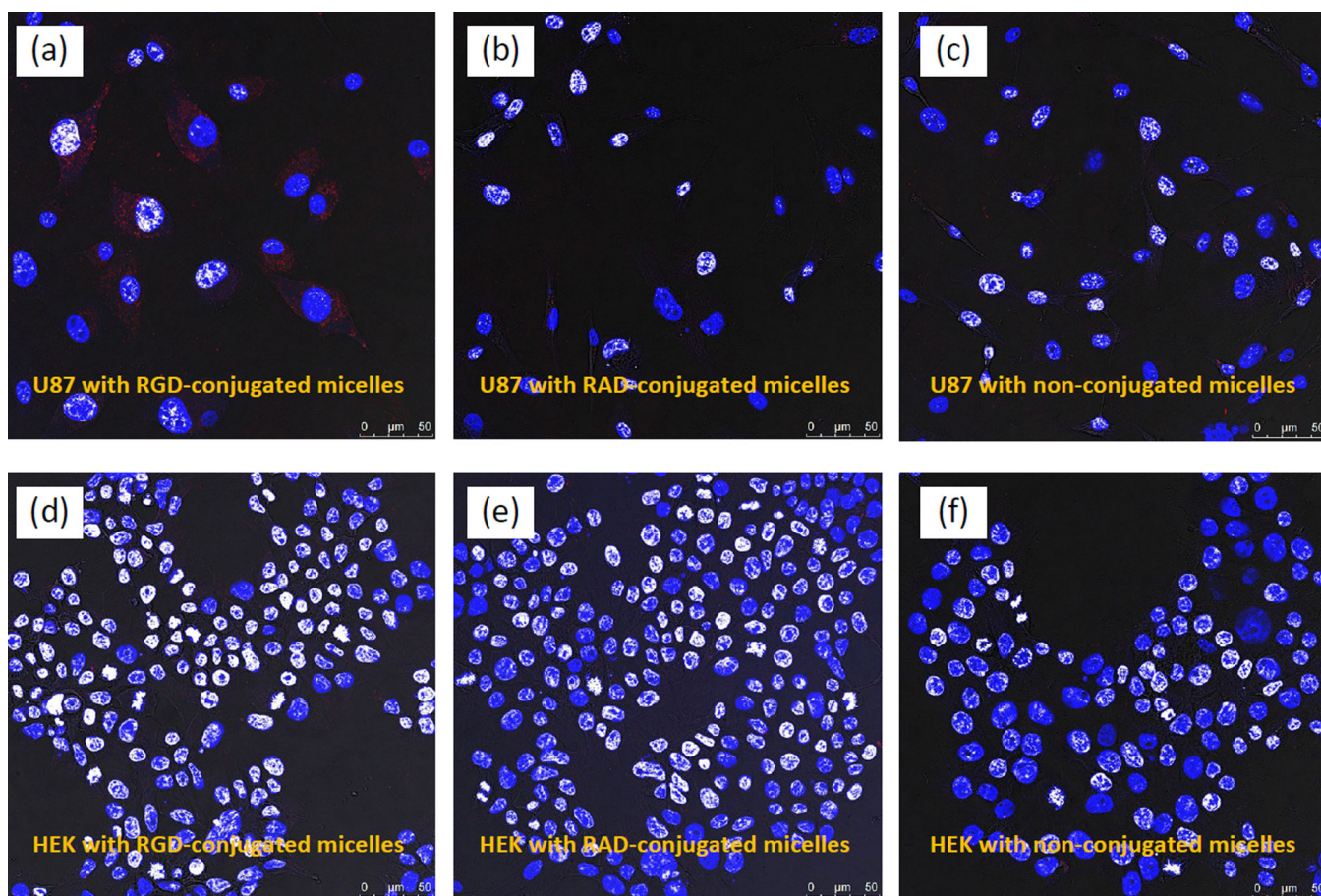
Figure 5.
Overlaid confocal images demonstrating the cellular uptake/internalization of RGD-conjugated, RAD-conjugated and non-conjugated micelles under the same dilution or concentration of micelles (25 times dilution from the conjugate stock) by U-87 and HEK-293 (Red color in images indicates the PL emission from micelles).
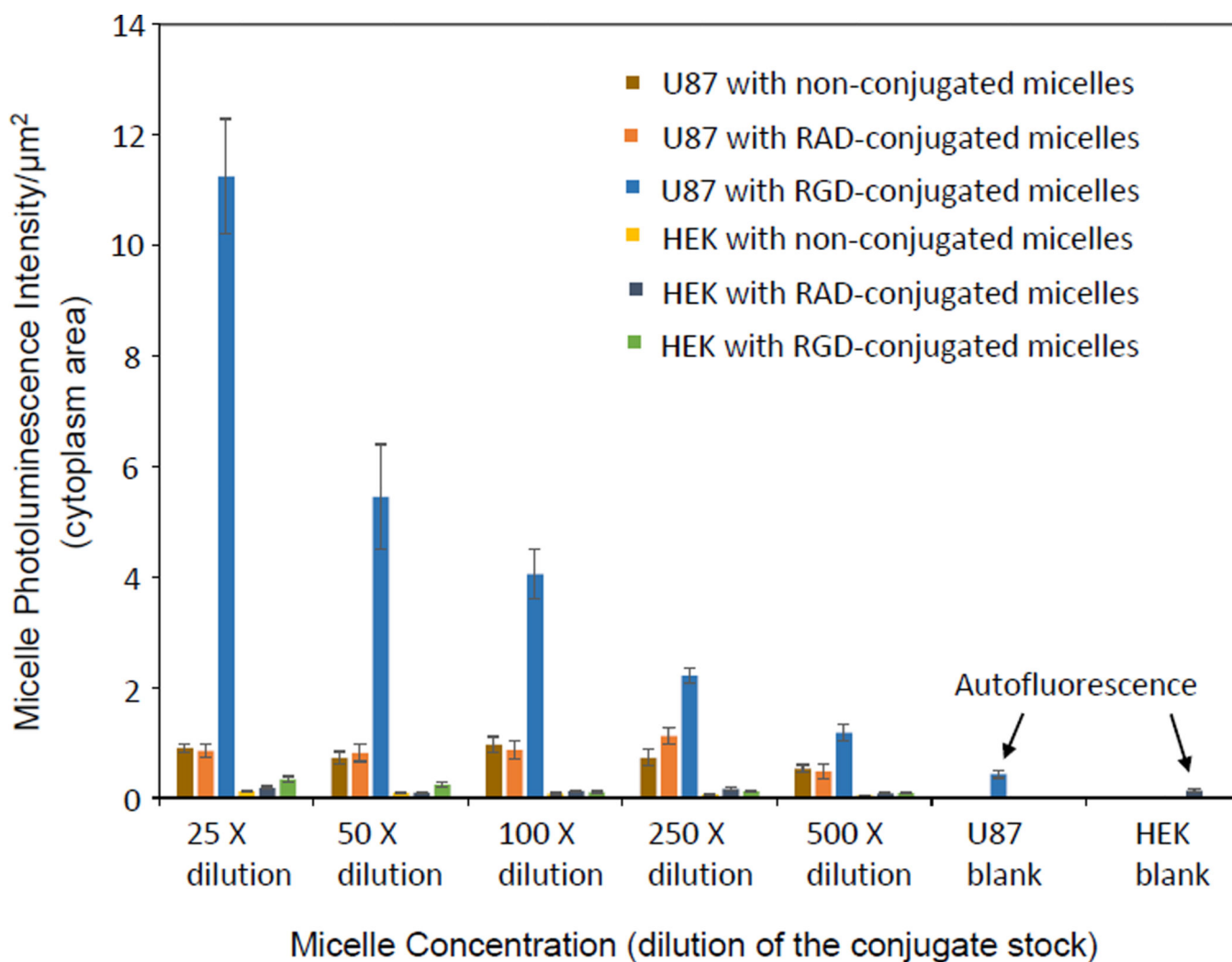
Figure 6.
Fluorescent intensity per unit area of cytoplasm for U-87 and HEK-293 cells incubated with non-conjugated micelles, RAD-conjugated micelles and RGD-conjugated micelles with different dilutions or concentrations. All *p* values for each comparison are less than 0.001.

Author Manuscript

Author Manuscript

Table 1

Element atomic ratio (EDX analysis) of AIS NCs and Cu:AIS NCs

	Measured Atomic Ratio by EDX			QY (%)
	Cu	Ag	In	S	
AIS	-	21.5	23.9	54.5	28.9
1.67% Cu:AIS	1.0	20.5	25.0	53.5	23.2
6.67% Cu:AIS	3.6	17.6	26.0	52.7	19.7

Author Manuscript

Author Manuscript

Table 2

PL decay parameters of Cu:AIS NCs and Cu:AIS/ZnS NCs

NCs	τ_1/ns	A_1	τ_2/ns	A_2	τ_{avg}/ns
AIS	49	51.6%	369	48.4%	329
1.67% Cu:AIS	62	45.2%	413	54.8%	374
6.67% Cu:AIS	66	44.8%	414	55.2%	374
AIS/ZnS	125	49.2%	416	50.8%	350
1.67% Cu:AIS/ZnS	131	41.7%	461	58.3%	405
6.67% Cu:AIS/ZnS	151	42.2%	499	57.8%	436